A moisture-enabled fully printable power source inspired by electric eels

Lu Yang[a], Feiyao Yang[a], Xu Liu[a], Ke Li[a], Yaning Zhou[a], Yangjian Wang[a], Tianhao Yu[a], Mengjuan Zhong[a], Xiaobing Xu[a], Lijuan Zhang[a], Wei Shen[a], and Di Wei[a,1]

[a]Beijing Graphene Institute, 100095 Beijing, China

Edited by Alexis T. Bell, University of California, Berkeley, CA, and approved January 21, 2021 (received for review November 6, 2020)

Great efforts have been made to build integrated devices to enable future wearable electronics; however, safe, disposable, and cost-effective power sources still remain a challenge. In this paper, an all-solid-state power source was developed by using graphene materials and can be printed directly on an insulating substrate such as paper. The design of the power source was inspired by electric eels to produce programmable voltage and current by converting the chemical potential energy of the ion gradient to electric energy in the presence of moisture. An ultrahigh voltage of 192 V with 175 cells in series printed on a strip of paper was realized under ambient conditions. For the planar cell, the mathematical fractal design concept was adapted as printed patterns, improving the output power density to 2.5 mW cm^{-3}, comparable to that of lithium thin-film batteries. A foldable three-dimensional (3D) cell was also achieved by employing an origami strategy, demonstrating a versatile design to provide green electric energy. Unlike typical batteries, this power source printed on flexible paper substrate does not require liquid electrolytes, hazardous components, or complicated fabrication processes and is highly customizable to meet the demands of wearable electronics and Internet of Things applications.

moisture-enabled electric power source | inkjet printing | graphene inks | ion gradient | electric eels

Future electronics call for wearable and even disposable power sources that can be customized to meet the demands of integrated systems; for example, flexible and disposable power sources are needed to provide energy for multifunctional contact lenses in real-time health monitoring applications (1). Among numerous manufacturing methods, printing shows great potential to build freeform products due to its geometric controllability, process flexibility, and cost-effectiveness (2). Printed energy storage devices such as lithium-ion batteries (3, 4) and alkaline batteries (5, 6) have been extensively studied to power next-generation devices. However, most of these energy storage systems contain hazardous or flammable components and thus cannot meet the safety and environmental requirements for green power sources, which are crucial for future disposable electronic devices.

Nature gives inspiration for many ideas in the search of alternative green power sources (7). Among numerous forms of energy in nature, the chemical potential energy of the ion gradient is the foundation of many living species and has attracted increasing research attention since the award of the 2003 Nobel Prize in Chemistry for ion channels in cell membranes (8). The electric eel is an excellent example of an electric power source utilizing ion gradients to generate high voltages and currents. As shown in Fig. 1*A*, each electrocyte in the electric organ has highly selective membranes that can produce transmembrane potential via the flux of small ions. The action potential from the Na^+ and K^+ ion gradient is 65 and 85 mV, respectively, which adds up in series and results in a total transcellular potential of ∼150 mV (9). Thousands of electrocytes in series and parallel arrangement can generate potential up to 600 V and peak current of 1 A (10). To extract electric energy from the ion gradient, various energy systems have been designed such as reverse electrodialysis (RED), which can extract electric energy from the mixing of sea and river water (11, 12). However, these RED systems usually rely on bulky pumping systems and large ion-exchange membrane stacks and thus are not suitable for portable applications. Recently, some novel power sources have been developed to utilize the chemical potential energy of the ion gradient, such as artificial electric organs (10), nanofluidic devices (13), and moist-electric generators (14, 15). Although some of these devices are portable, they still suffer from low voltage output or require a complicated fabrication process.

Herein, inspired by electric eels, we developed a fully printable all-solid-state power source based on graphene inks with an open-circuit voltage (OCV) up to 1.2 V for each cell, which is eight times higher than that of biological electric signals (9). The high voltage comes from the large cation concentration difference which is maintained by graphene oxide (GO) materials. GO materials are reported to have large salt intake, leading to highly concentrated solutions that are close to the saturation inside graphene capillaries, enable ultrafast ion permeation (16), and have been applied in adsorption (17) and selectively permeable membranes (18, 19). GO materials also have unimpeded water permeation capability (20), tunable ion-exchange properties (16, 21), and enhanced cation conductivity (22, 23) due to their unique two-dimensional (2D) nanofluidic channels, which are favorable for solid-state ionic conductors in humid environments. In the presence of water molecules, cations are transported from the high-concentration side to the low-concentration side, creating a potential difference. This directional ion migration is then

Significance

Future wearable and printable electronics call for scalable production of power sources that can provide green electric energy. The chemical potential energy of the ion gradient is ubiquitous in nature and is the foundation of many living species. Herein, inspired by electric eels, a new power source printed from graphene inks can convert the chemical potential energy of the ion gradient to electric output in the presence of moisture. An ultrahigh voltage of 192 V is achieved on a strip of paper substrate. Two- and three-dimensional cell structures are designed by adapting the mathematical fractal curves and a origami-folding strategy. The industrial-scale production of graphene materials coupled with the reproducibility of printing technology could open new scenarios of cost-effective graphene electronic devices.

Author contributions: D.W. designed research; L.Y., F.Y., X.L., K.L., Y.Z., and X.X. performed research; L.Y., F.Y., X.L., K.L., Y.Z., Y.W., T.Y., M.Z., and D.W. contributed new reagents/analytic tools; L.Y., L.Z., W.S., and D.W. analyzed data; and L.Y. and D.W. wrote the paper.

The authors declare no competing interest.

This article is a PNAS Direct Submission.

[1]To whom correspondence may be addressed. Email: weidi-cnc@pku.edu.cn.

This article contains supporting information online at https://www.pnas.org/lookup/suppl/doi:10.1073/pnas.2023164118/-/DCSupplemental.

Published April 12, 2021.

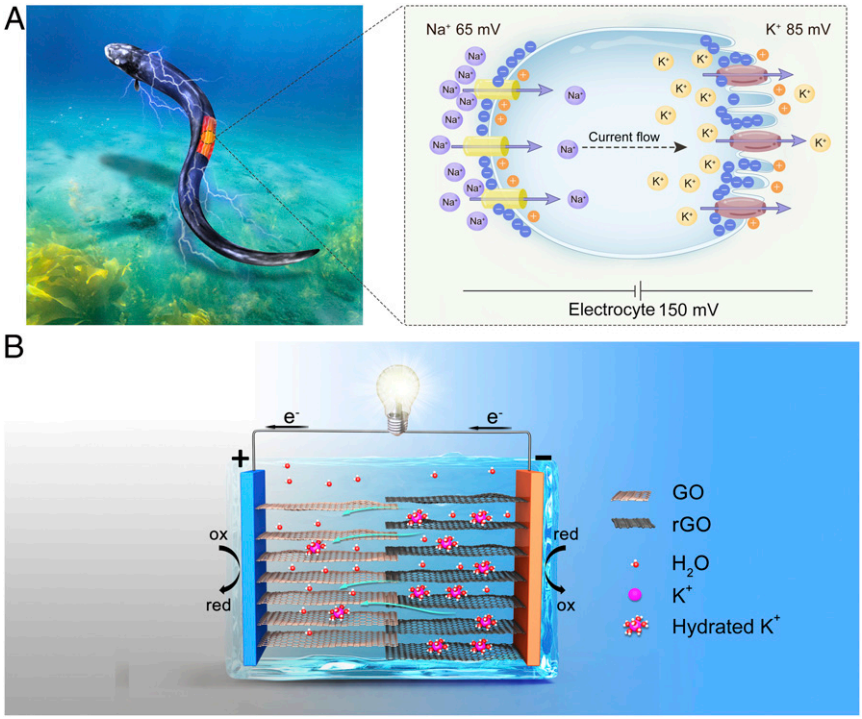

Fig. 1. Schematic of structures of the electric eel's electrocytes and the moisture-enabled power source. (*A*) Each electrocyte of the electric eel can generate 150 mV when stimulated via ion transportation of K^+ and Na^+ through highly selective ion channels on cell membranes. (*B*) The designed power source is composed of GO inks and rGO inks with different ion concentrations and a pair of silver electrodes. In the presence of moisture, the chemical potential energy of the ion gradient is converted to electric energy via directional ion migration and redox reactions and thus produces electric power.

converted to electron transportation at the surface of electrodes via redox reactions or charge adsorption, thus generating electric current output (Fig. 1*B*). When stored in low-moisture conditions, such as in a vacuum bag, a sealed container with desiccant and filled with dry N_2, or a climate-controlled facility with low humidity levels, there is limited ion transportation and therefore little to no self-discharge, ensuring a long shelf life unlike typical batteries (24). The cell is safe, disposable, and cost-effective, since all parts are inkjet printed onto paper to form an all-solid-state flexible power source, avoiding flammable and hazardous components. The geometric controllability of inkjet printing also allows a flexible cell pattern design (2). By optimizing the printing parameters, an ultrahigh voltage of 192 V was achieved on a small strip of paper under ambient conditions by connecting 175 cells in series. By adapting the mathematical space-filling curves as the printed pattern to increase the cell length (25, 26), the planar cell can achieve a short-circuit current of 170 μA and the power density can reach 2.5 mW cm^{-3} with energy density up to 0.41 mWh cm^{-3}, which is comparable to that of lithium thin-film batteries (27). The output voltage and current are readily adjustable by arranging well-defined patterns in parallel and series connections. A foldable three-dimensional (3D) cell using an origami pattern was also fabricated, demonstrating a versatile design strategy for printed electronics. This interdisciplinary work opens a novel design direction for utilizing ion gradients and offers a simple but effective method to provide scalable green electric power for practical applications.

Results

Cell Construction and Electric Output Performance. A printed cell was composed of two GO-based inks with different ion concentrations and a pair of silver electrodes. The GO in this paper was prepared with Hummers' method and purchased from Tanfeng Tech. Inc. After exfoliating graphite oxide with different chemical agents, abundant oxygen-containing functional groups were bound onto the surface of GO layers by noncovalent interactions (28). This negatively charged oxidized debris can not only improve GO's hydrophilic property but also promote cation transportation in nanochannels between the layered structure due to surface charges and capillary force (21, 23) and therefore enables GO to act as a solid-state ionic conductor in the presence of moisture. To introduce the large ion gradient, KOH was added to the GO solution, which is termed as reduced graphene oxide (rGO) inks in this study. K^+ was chosen due to its small hydrated ionic radius of 3.31 Å (29), which is lower than that of Li^+ or Na^+ and favorable for ion transportation under humidity. Recently, it was reported that the low ion charge and weakly bound hydration shells of K^+ also promote the entry of hydrated ions into nanochannels, leading to a higher permeation rate than that of Ca^{2+} or Mg^{2+} ions (18). In addition, a modest concentration of KOH would not affect the solubility of GO and the potassium salt would not crystalize or separate from GO when dried because GO was reported to undergo a series of deoxygenation reactions under alkaline conditions (30, 31), forming soluble salt solutions with large negatively charged GO sheets and small cations between layered structures. It should be noted that although the color of the solutions changed from light to dark brown, the reaction of GO with KOH at room temperature only partially removed the functional groups, which is proved in the following characterization results; thus, it is still soluble in water and should still have the properties of GO. To distinguish two GO-based inks, rGO in this paper refers to the GO deoxygenated by KOH. For GO ink, there is no added KOH. Although there might be some residue K^+ from the manufacturing process, the concentration is relatively low compared to that of rGO ink. The pair of silver electrodes was printed onto paper substrate, not only acting as current collectors but also participating in redox reactions to

promote the conversion of ionic current to electric current, which will be discussed in detail in the mechanism study below.

Although pure GO and rGO can exhibit similar electrochemical behaviors and produce voltage and current in the presence of moisture, the viscosity and surface tension of GO or rGO aqueous solutions without additives cannot satisfy the requirements for inkjet printing. Nafion is a polymer with high cation conductivity that will not hinder water permeation or react with GO (32, 33), and it is added to GO solutions to adjust the printability of GO ink. To tailor the rGO inks for inkjet printing, sodium dodecyl benzene sulfonate (SDBS) was added to the rGO solutions. SDBS is a common surfactant to reduce surface energy (34). Since SDBS is water soluble, it can coexist with KOH in rGO aqueous ink. The performance of a single cell by drop-casting from GO ink and rGO ink is illustrated in Fig. 2. The OCV of 1.2 V could be maintained for more than 90 h at ambient conditions (25 °C, relative humidity [RH] 10%) as shown in Fig. 2*A*. The OCV was eight times higher than that of biological electrocytes (9). The galvanostatic discharge curve at 25 °C and RH 70% showed a stable voltage output and is beneficial for practical applications (Fig. 2*B*).

Working Mechanism. To understand the working mechanism of this new type of electrochemical cell, various characterization techniques were employed to investigate the evolution of materials during the discharge process. The influence of additives should first be eliminated when investigating K^+ ion transport. GO and rGO solutions were first dispersed in water with an ultrasonic homogenizer to achieve uniform sheet-size distribution without polymers or surfactants. Then they were filtered to thin-film forms, and a separator was used to avoid the direct contact of GO and rGO in the sandwich cell structure during galvanostatic discharge. Raman spectroscopy was performed to study the disorder and defects in GO and rGO as shown in Fig. 3*A*. The disorder-induced band (D peak) was located near 1,350 cm^{-1} and the graphite band (G peak) was close to 1,580 cm^{-1} (31). The intensity ratio of two peaks (I_D/I_G) for rGO was 1.210, higher than that of 1.063 for pristine GO. This can be attributed to the reaction of KOH with functional groups in GO structures. By removing part of the oxygen-containing groups, GO structures might be broken down and cations left between GO layers, therefore increasing the disordered degree of GO. This is in consistent with the results of particle-size analysis (*SI Appendix*, Fig. S1 *A* and *B*). The size distribution of GO particles was more scattered after adding KOH. After discharge to 0 V, I_D/I_G of GO was 1.099, slightly higher than that of pristine GO (1.063). This suggests no major structural changes in GO; the small increase in disorder might be from the insertion of K^+ ions between layers. For the rGO side, I_D/I_G was 1.125 after discharge, lower than that of pristine rGO (1.210); this indicated a decrease in defects, which might be explained by the removal of some K^+ ions between layers or a series of reactions leading to the electrochemical reduction (31, 35).

Inductively coupled plasma (ICP) and X-ray diffraction (XRD) were applied to provide further evidence of cation transportation. Fig. 3*B* shows that the concentration of K^+ in GO increased from 1,596 to 5,419 ppm after discharge, and it provides direct evidence of cation transportation from rGO to GO. The interlayer spacing of GO increased from 7.7 to 8.5 Å by adding KOH, suggesting that K^+ ions exist between layered structures (Fig. 3*C*). After discharge, the interlayer spacing of GO increased to 8.9 Å as a result of K^+ ion insertion into GO layers during the process, while the interlayer spacing of rGO did not change much since only some cations were transported to the GO side.

To generate electricity output, the directional migration of cations from the GO to rGO side needs to be converted to electron transportation at the surface of electrodes. In RED systems, this is completed by redox reactions at anodes and cathodes with the participation of redox couples in electrolytes or oxygen and water molecules from the environment (36). In moisture-electric generators, this process is achieved via charge adsorption on the surface of electrodes without redox reactions (14, 15). To study this process in our system, gold was employed to exclude possible reactions from electrodes so they only acted as current collectors. The OCV of drop-casted cells decreased with increasing RH, which could be explained by the change in ion concentration with the change in moisture conditions (Fig. 4*A*). It should be noted that the SD of the OCV for a batch of identically prepared power sources was relatively small, as shown in the error bar in Fig. 4*A*, indicating good voltage output reproducibility. Compared to that of silver electrodes, the OCV of a cell with gold current collectors was higher at all tested humidity conditions. However, the discharge curves showed that the capacity of the cell with gold current collectors was significantly lower than that of the silver electrodes (Fig. 4*B*). Further cyclic voltammetry (CV) tests were carried out to study the electrochemical process. The CV curve of the cell with gold current collectors indicated no major redox reactions within the voltage window, while that of the silver electrodes showed obvious redox peaks and high reaction current during the charge and discharge process, indicating the participation of silver in the redox reactions (Fig. 4*C*). The redox peaks occured between 0.1 and 0.4 V, which coincided with the discharge voltage platform. These electrochemical test results suggest a different electrochemical process at the electrode surface. For cells with gold current

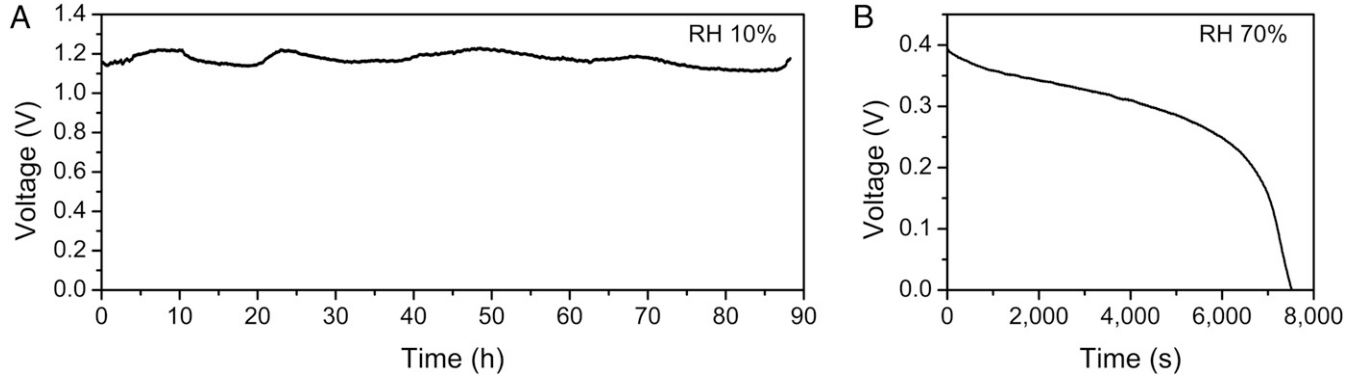

Fig. 2. Electrochemical performance of a drop-casted cell. (*A*) The OCV of a cell in an ambient environment (25 °C RH 10%). (*B*) Galvanostatic discharge performance at 0.1 μA at 25 °C RH 70%.

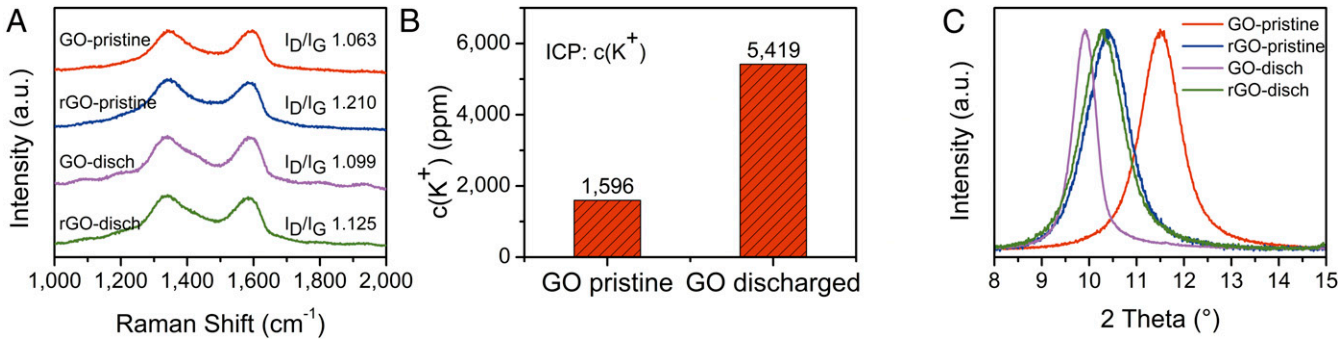

Fig. 3. Characterization of materials evolution of the discharge process. (*A*) Raman spectra of GO and rGO before and after discharge. (*B*) K^+ ion concentration in GO measured by ICP indicates cation transportation to GO during discharge. (*C*) XRD of GO and rGO suggests an interlayer spacing change.

collectors, there is no major redox reaction and the ion migration is converted to electron transportation via charge adsorption on the surface, similar to that of the moisture-electric generators (14, 15). For cells with silver electrodes, silver nanoparticles participate in the partially reversible redox reactions, similar to the process in RED systems (36). Since this is an open system, water or oxygen from the environment might participate in redox reactions. During the discharge process, oxygen might be reduced to water in an acidic environment on the GO side; silver might be oxidized to silver oxide under alkaline conditions on the rGO side, similar to the electrode reactions of silver–zinc batteries (37). These reactions are partially reversible as shown in the redox peaks in the CV curve, which is consistent with the cycling test results (*SI Appendix*, Fig. S2 *A* and *B*). Although the capacity decreased within 10 charge–discharge cycles, which might be due to the internal resistance, the results confirmed that our power source could be regenerated. The OCV of cells with gold current collectors came mainly from the high cation

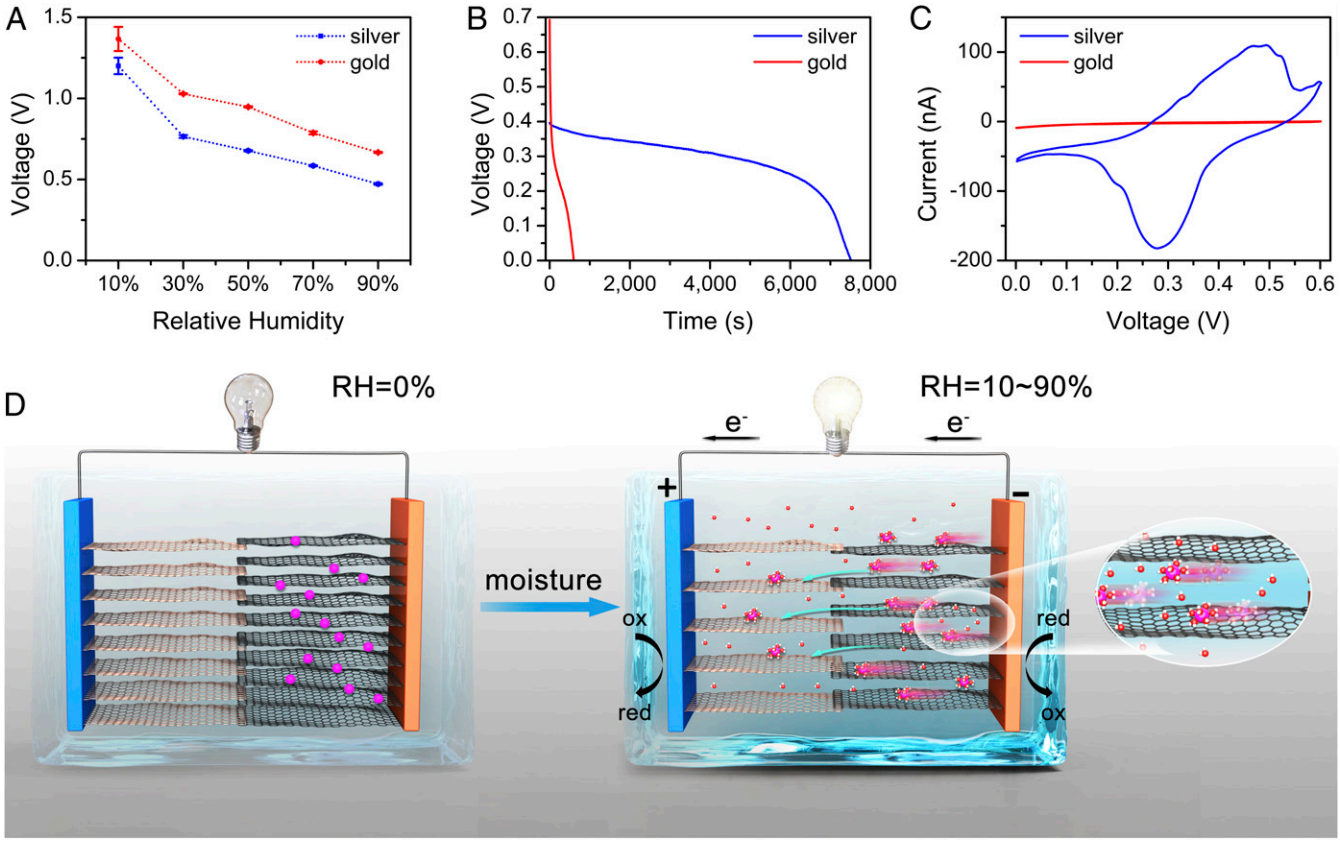

Fig. 4. Electrochemical tests of cells with gold current collectors and silver electrodes and the proposed working mechanism. (*A*) OCV of drop-casted cells with gold current collectors and silver electrodes at room temperature with different RH (error bar represents SD, $n = 3$). (*B*) Galvanostatic discharge performance at 0.1 μA at 25 °C RH 70%. (*C*) CV tests of cells at the slow scan rate of 0.1 mV s^{-1} (25 °C RH 70%). (*D*) Schematic of the cell working process. When exposed to an ambient environment, the interlayer spacing of GO and rGO increases with moisture absorption, forming nanochannels with a negative surface charge. Highly concentrated solutions were formed between rGO sheets. Hydrated cations were able to migrate from rGO to GO through these channels driven by ion gradient and capillary force, generating a potential difference. Redox reactions on the silver electrode surface then converted this directional ion migration to electron transportation, thus producing electric current.

concentration difference since there were no major redox reactions, and the OCV drop in cells with silver electrodes might be explained by the voltage loss introduced by redox reactions, which has been studied in RED systems (36). Theoretically, the Nernst equation is used to calculate this voltage loss introduced by redox reactions (38). However, since our cell is operating as an all-solid-state power source in a moisture environment without liquid electrolytes, the potential loss could only be estimated with the guide of the Nernst equation (*SI Appendix*, Fig. S3). The significant rise in discharge capacity for cells with silver electrodes might be explained by the steady conversion of ion migration to electron transportation via continuous redox reactions, while the charge adsorption on gold current collectors is limited by its surface conditions. Therefore, silver was selected as the electrode in our system not only to collect current but also to achieve better electric output performance.

The working mechanism of this new electrochemical cell is illustrated in Fig. 4*D*. When there was no moisture, the OCV was kept at 0 V in an Ar-filled glove box (*SI Appendix*, Fig. S4), since there was no electrolyte or ion transportation, mimicking the resting stage of electrocytes in electric eels. When exposed to a moisture environment, the interlayer spacing of GO and rGO rose with the increasing degree of hydration (39). Nanochannels were constructed within GO and rGO sheets with negative surface charges, which promote cation transportation but exclude anions (21, 23). Due to the large salt intake and unimpeded water permeation, highly concentrated solutions that were close to saturation were formed between 2D rGO sheets (16), maintaining a large ion concentration difference and enabling ultrafast ion permeation of hydrated K^+ from rGO to GO driven by the ion gradient and capillary force. The directional ion migration was then converted to electron transportation through redox reactions at the electrode surface, thus converting chemical potential energy to electric energy. In other words, the power source could be seen as a silver battery. The voltage came from the K^+ ion gradient between GO and rGO, and the current was provided by redox reactions on silver electrodes. The K^+ ion imbalance helps the diffusion of ions through aqueous electrolytes which are enabled by atmosphere moisture.

Inkjet Printing Design Parameters. With the understanding of the cell working mechanism, a fully printable power source can be fabricated via inkjet printing and optimized to achieve better electrochemical performance (Fig. 5). A pair of silver electrodes was first printed onto paper substrate with a thickness of 4 μm (*SI Appendix*, Fig. S5*A*). GO and rGO inks need to be adjusted in order to be printed through a nozzle with an 80-μm diameter. As mentioned before, the viscosity and surface tension of GO and rGO inks must be optimized to satisfy the requirements of inkjet printers. Although pure GO solution can also provide similar output performance, the hydrophilic nature of GO will attract rGO solution and thus lower the cation concentration difference or even cause a short circuit between electrodes. As a polymer with high cation conductivity, Nafion was added to GO solutions to adjust the ink printability. The viscosity of optimized GO ink was 8.05 cP and the contact angle with the photo paper substrate was 32.6° (*SI Appendix*, Fig. S6*A*), suitable for inkjet printing, as shown by the optical image of a printed strip with GO ink on paper substrate (Fig. 5*B*). The thickness of one printed GO ink layer was about 300 nm (*SI Appendix*, Fig. S5*B*). For the rGO ink, the viscosity and surface tension were adjusted with water-soluble surfactant SDBS, since the polymer tends to agglomerate with rGO and block the nozzle. The optimized rGO ink had a viscosity of 2.45 cP and a contact angle of 25.1° (*SI Appendix*, Fig. S6*B*) and had good printability, as shown in the optical image of a printed strip with rGO ink (Fig. 5*C*). The thickness of one printed rGO ink layer was about 50 nm (*SI Appendix*, Fig. S5*C*).

Moreover, the printing pattern parameters are crucial for the output performance of a cell. The thickness of a cell (H) is controlled by the repeating times of printing. The overlap width of GO and rGO inks (L_1) is designed to ensure the contact of GO and rGO, while the distance of printed inks to electrodes (L_2) can prevent the electric short circuit. These printing parameters have significant influence on OCV and short-circuit current (I_{sc}). Optimizing these parameters could improve the cell output performance, and detailed analysis is shown in *SI Appendix*, Fig. S7. Considering the capability of our printing facility and experiment time, a thickness (H) of 30 layers, overlap width (L_1) of 0.5 mm, and distance to electrode (L_2) of 0.5 mm were chosen as the optimized design parameters for the

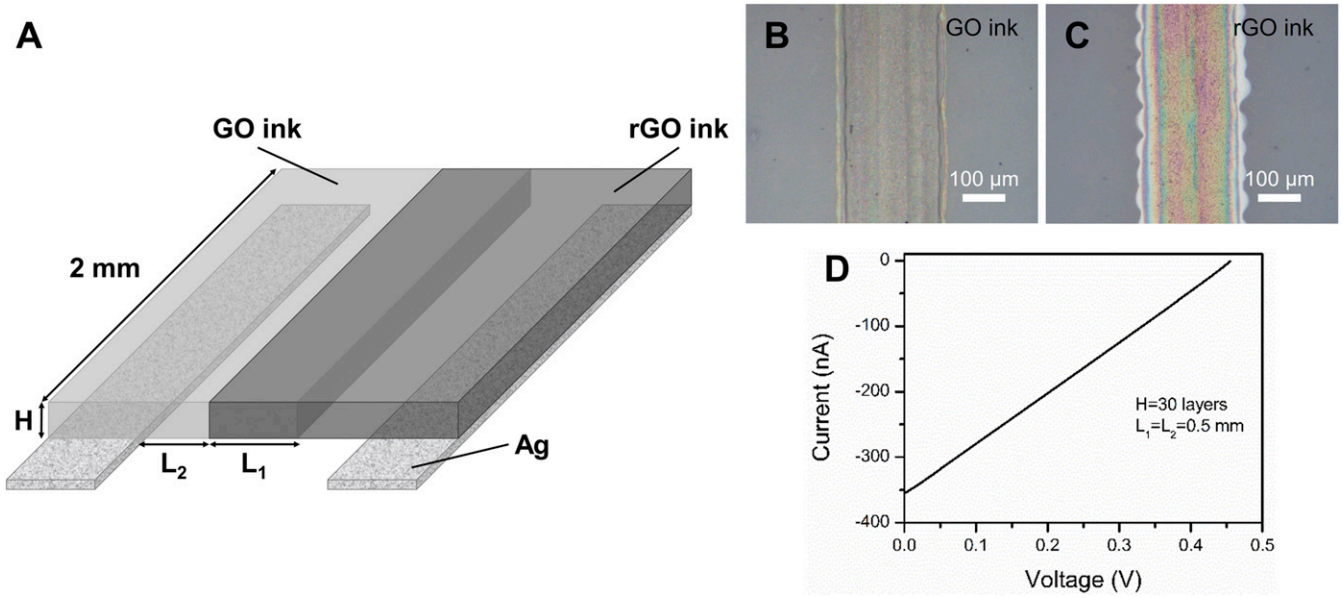

Fig. 5. Schematic of inkjet-printed cell structures and cell performance with optimized parameters. (*A*) The structure of a printed cell. (*B*) GO ink and rGO ink were printed onto paper substrate with silver electrodes. (*C*) Optical microscope images of printed strips reflect the good printability of GO and rGO inks. (*D*) I-V characteristic of the cell with optimized thickness (H), overlap width (L_1), and distance to electrodes (L_2) at 25 °C RH 70%.

following demonstration. As shown in Fig. 5*D*, a cell (0.2 cm × 0.25 cm × 13 μm) with optimized parameters had an OCV of 0.455 V and a short circuit current of 0.355 μA (25 °C, RH 70%). The maximum power density was calculated to be 0.6 mW cm^{-3} and the energy density was 0.41 mWh cm^{-3} (*SI Appendix*, Fig. S8 *A* and *B*). Owing to the geometric controllability and batch-to-batch reproducibility of the inkjet printing method, this output performance of the power source could be achieved in large-scale production.

Demonstration of Applications. Similar to electric eels, the output performance of the power source can be adjusted by series and parallel connections, since inkjet printing has the advantage of a flexible pattern design. To highlight the high-voltage advantage of the power source, 175 cells in series connection were printed onto a strip of paper substrate with optimized parameters (Fig. 6*A* and Movie S1). An ultrahigh voltage of 192 V was achieved under ambient conditions (RH 15% in Beijing), and the flexibility was demonstrated in Movie S2 to stress the potential applications in future wearable electronic systems. To the best of our knowledge, this is the highest voltage achieved in such a small area by printable power sources that utilize the ion gradient.

Larger output current can be realized by increasing the length of a planar cell (parallel connection). In fractal geometry, a space-filling curve is a continuous curve that can completely fill up higher-dimensional spaces such as a 2D unit square; it is a curve with an infinite length property on a finite area. The mathematical concept of space-filling curves has been employed by electronics to realize stretchable device design (26) and by capacitors to improve capacitance (25). Herein, to increase the cell length, a Peano curve in fractal geometry was adapted as the printed pattern, since it is reported to have a larger slot length relative to side length compared to other space-filling curves (25), meaning a larger cell length per unit area. As shown in Fig. 6*B*, the space was separated into two regions with a continuous curve and GO and rGO inks were printed to fill each region with the optimized overlap width (L_1) of 0.5 mm. The printed cell with a Peano curve pattern had an OCV of 0.44 V and I_{sc} of 37.4 μA on a small area (2.05 cm × 2.35 cm) and the maximum output power density was 0.7 mW cm^{-3} (25 °C RH 70%, *SI Appendix*, Fig. S9 *A* and *B*). The power density was approximately the same as that of a smaller cell at the same environmental conditions, suggesting no obvious power loss when scaled up. At a higher RH of 90%, the short-circuit current of the cell could reach up to 170 μA and the maximum power density was 2.5 mW cm^{-3} (Fig. 6*C*), comparable to that of lithium thin-film batteries (27).

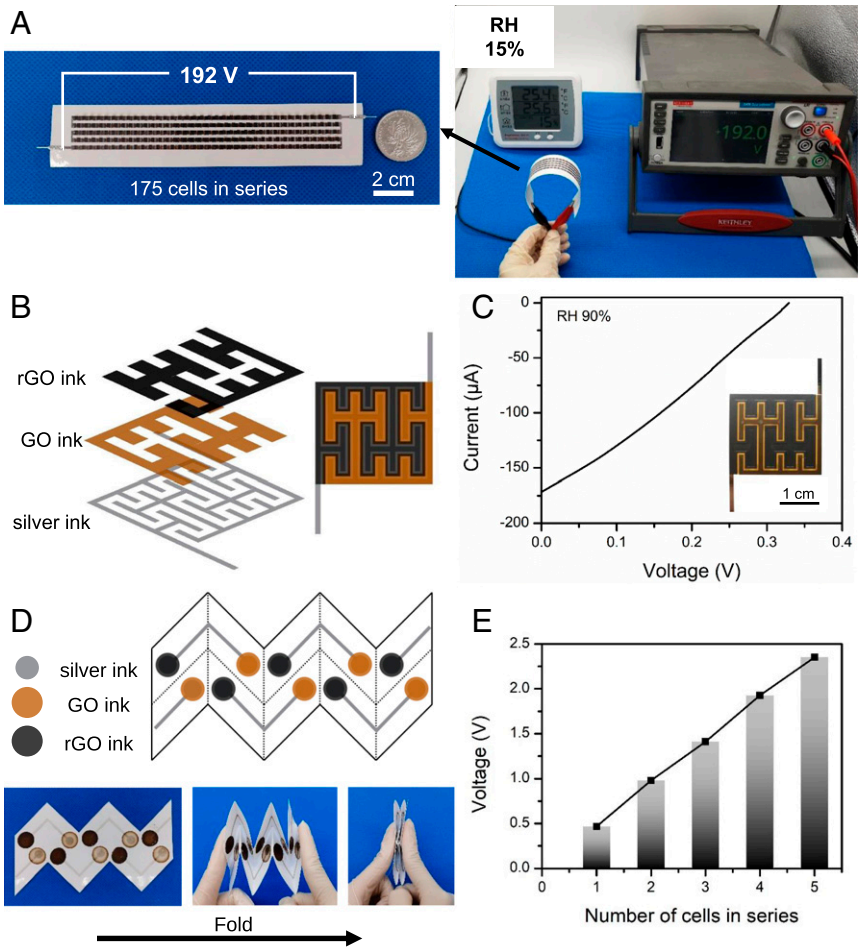

Fig. 6. Demonstration of applications. (*A*) Photographs of printed cells in series connection. One hundred seventy-five cells were printed onto a strip of flexible paper substrate and exhibited an ultrahigh OCV of 192 V under ambient conditions (RH 15% in Beijing). (*B*) The Peano curve was adapted as a printed pattern and the space was separated by a continuous curve into two regions filled with printed GO and rGO inks. (*C*) The output performance of a printed cell with the Peano curve pattern (25 °C RH 90%). (*Inset*) Photograph of the printed cell. (*D*) The foldable cell design with the *Miura-ori* strategy. (*E*) The OCV of foldable cells connected in series (25 °C RH 70%).

To further emphasize the design flexibility and diversified cell structures, a 3D foldable cell was fabricated with an origami-folding strategy. Three-dimensional architecture design could extend the functionality of devices and systems beyond those achievable with planar 2D platforms, such as the 3D chip design to extend beyond Moore's law in a vertical direction (40). Three-dimensional structures inspired by origami have been demonstrated to extend applications in complicated conditions and improve the performance of energy devices such as deformable lithium-ion batteries (41), 3D solar steam generators (42), and reconfigurable moisture-electric generators (43). We employed the *Miura-ori* folding strategy to simultaneously stack a series of thin films from a 2D to 3D structure in a single motion, which has been applied in various fields such as unfolding solar panels in space. As shown in Fig. 6*D*, a series of five cells on paper substrate with a *Miura-ori* design was fabricated with drop-casting GO and rGO inks. The cells can be activated by self-registered mechanical contact, while avoiding self-discharge before contact. The OCV of foldable cells increased linearly with the increasing number of connected cells (Fig. 6*E*). The cells could also be printed on both sides of the paper substrate, owing to the feasibility of the printing technology, thus further enhancing the output performance and providing a versatile design for future printed electronic circuits.

Discussion

In summary, we report a moisture-enabled bioinspired and all-solid-state green power source based on graphene inks via printing technology. The mechanism study shows that the chemical potential energy of the ion gradient is converted to electric energy via cation transportation and redox reactions in the presence of water molecules. The power source can maintain the OCV up to 1.2 V under ambient conditions, and an ultrahigh voltage of 192 V was achieved on a small strip of paper. The short-circuit current of 170 μA and power density up to 2.5 mW cm^{-3} was achieved utilizing the concept of space-filling curves. The output performance arises from the optimized geometric design realized by inkjet printing and the unique properties of GO, such as highly concentrated solutions in graphene capillaries, unimpeded water permeation, tunable ion-exchange properties, and enhanced cation conductivity. The output performance can also be flexibly adjusted by cell pattern and connections owing to geometric controllability and versatility of the printing method. The industrial-scale production of GO combined with the reproducibility of printing technology could open a new scenario of cost-effective graphene electronic devices. By employing a foldable origami design, the cell structure was transformed from 2D to 3D in a single motion, extending the potential application of printed electronics. Although the performance is comparable to lithium thin-film batteries, it might be further improved by precise tailoring of functional groups in GO structures and interlayer spacing to increase the ion concentration and ion transportation speed (18). This work is an example of interdisciplinary studies, which is inspired by biological phenomena in electric eels, realized by unique properties of GO materials and optimized by the mathematical fractal cell pattern and the origami folding method. This new design strategy opens a promising pathway for providing green electric energy and could be applied in scalable production of safe, disposable, and cost-effective power sources for the Internet of Things or other future wearable and disposable electronics.

Materials and Methods

Materials and Ink Preparation. GO solution was purchased from Tanfeng Tech. Inc. with a concentration of 10 mg mL^{-1}. Nafion was purchased from Sigma-Aldrich with a concentration of 5 wt. %. Silver ink was purchased from Sigma-Aldrich with 30–35 wt. % silver nanoparticles. GO ink was prepared by first dispersing 2 mg mL^{-1} GO aqueous solution with an ultrasonic homogenizer to achieve the desired sheet-size distribution and then adding Nafion with a 1:1 (vol/vol) ratio. rGO ink was prepared by first dispersing 5 mg mL^{-1} GO solution with an ultrasonic homogenizer and then adding 0.1 mol L^{-1} KOH and 0.4 mg mL^{-1} SDBS. All inks were uniformly dispersed with ultrasonication for 30 min before printing.

Cell Construction. For the mechanism study, 1 mg mL^{-1} GO-dispersed solution was first vacuum filtered to form a flexible thin film and dried in a vacuum. For the rGO side, as-obtained GO film was immersed in 0.1 mol L^{-1} KOH solution overnight at room temperature and then dried in a vacuum. To fabricate a cell with a sandwich structure, GO film and rGO film were clamped between two stainless-steel plates as current collectors and Celgard film was used as a separator to avoid direct contact. For drop-casted samples, first GO and then rGO inks were dropped onto polyethylene glycol terephthalate substrate with printed silver strips as electrodes or sputtered gold strips as current collectors (0.2 cm × 0.25 cm). Samples were dried overnight at room temperature at low humidity (RH lower than 1%). For inkjet printing, an RDLab-1C printer with a nozzle diameter of 80 μm was used. All inks were filtered prior to inkjet printing to avoid nozzle blockage. Silver ink was first printed onto photo paper substrate; GO and rGO inks were then printed onto silver electrodes with the designed pattern, respectively. For a foldable cell, GO and rGO inks were drop-casted onto paper substrate with patterned silver electrodes and then dried at room temperature.

Characterization. Raman spectra were collected with the LabRAM HR Evolution (Horiba) with a 532-nm laser. ICP (Thermo iCAP7200 DUO) was employed to measure cation concentration. XRD was tested with a Bruker D8 ADVANCE system with Cu Kα source. Particle-size analysis was measured with BLUEWAVE S3500 (Microtrac) with a 408-nm laser. Contact angle was measured with an optical tensiometer (Biolin THETA). Ink viscosity was measured with a rheometer (AMETEK Brookfield) at room temperature. The height profile was obtained with a white-light interferometric microscope (Nikon BW-S501).

Electrochemical Tests. All measurements were carried out with an electrochemical workstation (Multi Autolab M204), except the ultrahigh voltage measurements (Keithley 2450 source meter). Temperature and RH were controlled with an environmental simulation test chamber (Vötsch Technik). The galvanostatic discharge curve was obtained at 0.1 μA and the current–voltage characteristic was measured by potentiostatic linear sweep voltammetry from c OCV to 0 V at 10 mV s^{-1}. CV tests were carried out with the scan rate of 0.1 mV s^{-1} within the voltage window of 0 to 0.6 V.

Data Availability. All study data are included in the article and/or supporting information.

ACKNOWLEDGMENTS. This work was supported by Beijing Municipal Science & Technology Commission Grant No. Z181100004818004, Grant No. Z181100001018029, and Grant No. Z191100006119027. We also appreciate the technical assistance from the Beijing Graphene Institute Characterization & Quality Assurance Center.

1. J. Park *et al.*, Soft, smart contact lenses with integrations of wireless circuits, glucose sensors, and displays. *Sci. Adv.* **4**, eaap9841 (2018).
2. F. Zhang *et al.*, 3D printing technologies for electrochemical energy storage. *Nano Energy* **40**, 418–431 (2017).
3. K. Sun *et al.*, 3D printing of interdigitated Li-ion microbattery architectures. *Adv. Mater.* **25**, 4539–4543 (2013).
4. S.-H. Kim *et al.*, Printable solid-state lithium-ion batteries: A new route toward shape-conformable power sources with aesthetic versatility for flexible electronics. *Nano Lett.* **15**, 5168–5177 (2015).
5. G. A. Ghiurcan, C.-C. Liu, A. Webber, F. H. Feddrix, Development and characterization of a thick-film printed zinc-alkaline battery. *J. Electrochem. Soc.* **150**, A922–A927 (2003).
6. A. M. Gaikwad, D. A. Steingart, T. Nga Ng, D. E. Schwartz, G. L. Whiting, A flexible high potential printed battery for powering printed electronics. *Appl. Phys. Lett.* **102**, 233302 (2013).
7. M. S. Dresselhaus, I. L. Thomas, Alternative energy technologies. *Nature* **414**, 332–337 (2001).
8. D. A. Doyle *et al.*, The structure of the potassium channel: Molecular basis of K^+ conduction and selectivity. *Science* **280**, 69–77 (1998).
9. R. D. Keynes, H. Martins-Ferreira, Membrane potentials in the electroplates of the electric eel. *J. Physiol.* **119**, 315–351 (1953).
10. T. B. H. Schroeder *et al.*, An electric-eel-inspired soft power source from stacked hydrogels. *Nature* **552**, 214–218 (2017).

11. R. E. Pattle, Production of electric power by mixing fresh and salt water in the hydroelectric pile. *Nature* **174**, 660 (1954).
12. B. E. Logan, M. Elimelech, Membrane-based processes for sustainable power generation using water. *Nature* **488**, 313–319 (2012).
13. K. Xiao, L. Jiang, M. Antonietti, Ion transport in nanofluidic devices for energy harvesting. *Joule* **3**, 2364–2380 (2019).
14. Y. Huang *et al*., All-region-applicable, continuous power supply of graphene oxide composite. *Energy Environ. Sci.* **12**, 1848–1856 (2019).
15. X. Liu *et al*., Power generation from ambient humidity using protein nanowires. *Nature* **578**, 550–554 (2020).
16. R. K. Joshi *et al*., Precise and ultrafast molecular sieving through graphene oxide membranes. *Science* **343**, 752–754 (2014).
17. S. Wang, H. Sun, H. M. Ang, M. O. Tadé, Adsorptive remediation of environmental pollutants using novel graphene-based nanomaterials. *Chem. Eng. J.* **226**, 336–347 (2013).
18. J. Abraham *et al*., Tunable sieving of ions using graphene oxide membranes. *Nat. Nanotechnol.* **12**, 546–550 (2017).
19. Q. Yang *et al*., Ultrathin graphene-based membrane with precise molecular sieving and ultrafast solvent permeation. *Nat. Mater.* **16**, 1198–1202 (2017).
20. R. R. Nair, H. A. Wu, P. N. Jayaram, I. V. Grigorieva, A. K. Geim, Unimpeded permeation of water through helium-leak-tight graphene-based membranes. *Science* **335**, 442–444 (2012).
21. L. Chen *et al*., Ion sieving in graphene oxide membranes via cationic control of interlayer spacing. *Nature* **550**, 380–383 (2017).
22. K. Raidongia, J. Huang, Nanofluidic ion transport through reconstructed layered materials. *J. Am. Chem. Soc.* **134**, 16528–16531 (2012).
23. A. R. Koltonow, J. Huang, Ionic transport. Two-dimensional nanofluidics. *Science* **351**, 1395–1396 (2016).
24. A. Du Pasquier, I. Plitz, S. Menocal, G. Amatucci, A comparative study of Li-ion battery, supercapacitor and nonaqueous asymmetric hybrid devices for automotive applications. *J. Power Sources* **115**, 171–178 (2003).
25. T. Moselhy, H. Ghali, H. F. Ragaie, H. Haddara, "Investigation of space filling capacitors" in Proceedings of the 12th IEEE International Conference on Fuzzy Systems (Cat. No. 03CH37442) (IEEE, Cairo Egypt, 2003), pp. 287–290.
26. J. A. Fan *et al*., Fractal design concepts for stretchable electronics. *Nat. Commun.* **5**, 3266 (2014).
27. D. Pech *et al*., Ultrahigh-power micrometre-sized supercapacitors based on onion-like carbon. *Nat. Nanotechnol.* **5**, 651–654 (2010).
28. V. R. Coluci *et al*., Noncovalent interaction with graphene oxide: The crucial role of oxidative debris. *J. Phys. Chem. C* **118**, 2187–2193 (2014).
29. E. R. Nightingale, Phenomenological theory of ion solvation. Effective radii of hydrated ions. *J. Phys. Chem.* **63**, 1381–1387 (1959).
30. X. Fan *et al*., Deoxygenation of exfoliated graphite oxide under alkaline conditions: A green route to graphene preparation. *Adv. Mater.* **20**, 4490–4493 (2008).
31. S. Pei, H.-M. Cheng, The reduction of graphene oxide. *Carbon* **50**, 3210–3228 (2012).
32. K. A. Mauritz, R. B. Moore, State of understanding of nafion. *Chem. Rev.* **104**, 4535–4585 (2004).
33. D. Wei, Writable electrochemical energy source based on graphene oxide. *Sci. Rep.* **5**, 15173 (2015).
34. B. R. Priya, H. J. Byrne, Investigation of sodium dodecyl benzene sulfonate assisted dispersion and debundling of single-wall carbon nanotubes. *J. Phys. Chem. C* **112**, 332–337 (2008).
35. S. J. An *et al*., Thin film fabrication and simultaneous anodic reduction of deposited graphene oxide platelets by electrophoretic deposition. *J. Phys. Chem. Lett.* **1**, 1259–1263 (2010).
36. J. Veerman, M. Saakes, S. J. Metz, G. J. Harmsen, Reverse electrodialysis: Evaluation of suitable electrode systems. *J. Appl. Electrochem.* **40**, 1461–1474 (2010).
37. S. Berchmans *et al*., An epidermal alkaline rechargeable Ag–Zn printable tattoo battery for wearable electronics. *J. Mater. Chem. A Mater. Energy Sustain.* **2**, 15788–15795 (2014).
38. A. J. Bard, L. R. Faulkner, *Electrochemical Methods: Fundamentals and Applications* (John Wiley & Sons, ed. 2, 2000).
39. A. Lerf *et al*., Hydration behavior and dynamics of water molecules in graphite oxide. *J. Phys. Chem. Solids* **67**, 1106–1110 (2006).
40. W. R. Davis *et al*., Demystifying 3D ICs: The pros and cons of going vertical. *IEEE Des. Test Comput.* **22**, 498–510 (2005).
41. Z. Song *et al*., Origami lithium-ion batteries. *Nat. Commun.* **5**, 3140 (2014).
42. S. Hong *et al*., Nature-inspired, 3D origami solar steam generator toward near full utilization of solar energy. *ACS Appl. Mater. Interfaces* **10**, 28517–28524 (2018).
43. C. Yang, Y. Huang, H. Cheng, L. Jiang, L. Qu, Rollable, stretchable, and reconfigurable graphene hygroelectric generators. *Adv. Mater.* **31**, e1805705 (2019).